CALCIUM-INDUCED ASYMMETRICAL BEATING OF TRITON-DEMEMBRANATED SEA URCHIN SPERM FLAGELLA

C. J. BROKAW

From the Division of Biology, California Institute of Technology, Pasadena, California 91125

ABSTRACT

Asymmetrical bending waves can be obtained by reactivating demembranated sea urchin spermatozoa at high Ca^{2+} concentrations. Moving-film flash photography shows that asymmetrical flagellar bending waves are associated with premature termination of the growth of the bends in one direction (the reverse bends) while the bends in the opposite direction (the principal bends) grow for one full beat cycle, and with unequal rates of growth of principal and reverse bends. The relative proportions of these two components of asymmetry are highly variable. The increased angle in the principal bend is compensated by a decreased angle in the reverse bend, so that there is no change in mean bend angle; the wavelength and beat frequency are also independent of the degree of asymmetry. This new information is still insufficient to identify a particular mechanism for Ca^{2+}-induced asymmetry.

When a developing bend stops growing before initiation of growth of a new bend in the same direction, a modification of the sliding between tubules in the distal portion of the flagellum is required. This modification can be described as a superposition of synchronous sliding on the metachronous sliding associated with propagating bending waves. Synchronous sliding is particularly evident in highly asymmetrical flagella, but is probably not the cause of asymmetry. The control of metachronous sliding appears to be unaffected by the superposition of synchronous sliding.

KEY WORDS calcium · flagella · microtubules · motility · spermatozoa

A variety of situations has been found in which the movements of cilia and flagella can be modified, in vitro and presumably in vivo, by free Ca^{2+} ion concentrations in the range of 10^{-7} to 10^{-5} M. In the case of sea urchin spermatozoa, reactivated demembranated spermatozoa swim in circular paths of decreasing radius as the Ca^{2+} concentration is increased (12) and the flagellar beat pattern becomes highly asymmetrical. No functional significance for this behavior is known for sea urchin spermatozoa, but in other simple spermatozoa chemotactic responses may involve a similar development of asymmetrical flagellar beating (26). An inverse effect of Ca^{2+} has been reported for *Chlamydomonas* flagella (23). In *Crithidia* flagella, Ca^{2+} appears to control the direction of propagation of bends along the flagellum (22). In cilia, Ca^{2+} has been shown to determine the direction of the ciliary effective stroke in *Paramecium* (27) and to cause ciliary arrest in lamellibranch gill cilia (34). Machemer (25) has proposed a model for differential control of ciliary dyneins by Ca^{2+} and Mg^{2+} ions to explain the responses observed with

Paramecium cilia, but the extent to which these Ca^{2+}-mediated responses involve similar mechanisms and axonemal components is completely unknown.

Understanding of the mechanism of control by Ca^{2+} is made more difficult by the fact that we still lack an adequate understanding of the basic mechanisms by which the active sliding process in flagella and cilia operates and is controlled to produce oscillation and an appropriate pattern of propagated bending. Conversely, we might hope that information about the manner in which Ca^{2+} modifies beating might contribute to an understanding of these basic mechanisms. With this goal, a detailed examination of asymmetrical bending waves in live echinoderm sperm flagella was begun by Goldstein (19) and is now extended to Ca^{2+}-induced asymmetry of Triton-demembranated flagella. A preliminary report of some of these results has been given by Brokaw and Goldstein (11).

MATERIALS AND METHODS

Spermatozoa were obtained from the sea urchin, *Strongylocentrotus purpuratus*, by KCl injection, diluted slightly with 0.5 M NaCl, and stored on ice until used. All subsequent procedures and measurements with demembranated spermatozoa were carried out at 18°C.

Spermatozoa were demembranated for 30 s in Triton extraction solution (12) containing either 2 mM $CaCl_2$ or no $CaCl_2$, and then diluted ~1:100 with reactivation solution. The reactivation solutions used for these experiments all contained 0.25 M KCl, 20 mM Tris buffer, 2 mM dithiothreitol, 2% polyethylene glycol, 0.2% methyl cellulose (Fisher M-281, 4000 cP, Fisher Scientific Co., Pittsburgh, Penn.), 0.10 M ATP (Boehringer-Mannheim Biochemicals, Indianapolis, Ind.) and 2.0 mM of either EGTA or EDTA. Calculated amounts of $CaCl_2$ (from a stock solution made by dissolving $CaCO_3$ in HCl) and $MgSO_4$ were added to give the desired Ca^{2+} concentration and a Mg^{2+} concentration of 3.0 mM. Na_2SO_4 was added as required to eliminate differences in SO_4^{2-} concentration between solutions of different Ca^{2+} concentration; most solutions had a total SO_4^{2-} concentration of ~5 mM. The pH was adjusted to 8.2. The reactivation solutions had an apparent viscosity of ~7 cP (3). These reactivation solutions were designed to match the capabilities of the photographic system; the relatively low ATP concentration gives a beat frequency of ~10 Hz, the increased viscosity causes a wavelength reduction which compensates for the increased wavelength obtained when the beat frequency is reduced at lower ATP concentrations (7) and the relatively high Mg^{2+} concentration helps to maintain the amplitude of the bending waves at increased viscosity (15).

Except as noted, all measurements were obtained from photographs of spermatozoa swimming freely next to the lower glass surface of a covered well slide (9). Whenever necessary, the glass surface was rinsed with a solution containing a few drops of Siliclad (Clay-Adams, Inc., Parsippany, N. Y.) in 100 ml of glass distilled water, and polished with a pad of Kimwipes, to obtain an optically clean surface with minimal sperm adhesion. Photographs for measurement of wave parameters in the sperm sample were obtained by multiple-flash photography, using five flashes with the flash frequency adjusted to exactly four times the beat frequency (9). The adjustment of the flash frequency becomes very difficult when the spermatozoa are swimming in small circles with highly asymmetrical bending waves, and this limits the accuracy of the frequency measurements at high degrees of asymmetry. Photographs for detailed analysis of waveforms were taken at flash rates up to 100 Hz, using a Robot Star II 35-mm camera (Robot Foto und Electronic, Dusseldorf, Germany) which was modified so that the spring motor transported the film continuously during the time that the shutter was open. This camera achieves higher film transport rates than the camera used for moving-film photography of sperm flagella by Goldstein (18, 19) and permits the use of high flash rates without the expense of a pin-registering high speed 35-mm cine camera. Photographs were taken on Kodak Tri-X 35-mm film, developed in Acufine for 10 min at 26°C, and examined and measured on a Kodak Recordak microfilm viewer. Other details of these procedures have been recorded elsewhere (7, 9, 16).

To photograph spermatozoa during exposure to CO_2, an open drop preparation was used (9), with a × 16 objective. The pH of the reactivation solutions was increased to 8.4, to increase the sensitivity of the demembranated spermatozoa to CO_2 (9, 14), and a CO_2-N_2 mixture containing 10–20% CO_2 was directed over the surface of the drop. Spermatozoa swimming at the air-water interface were photographed.

RESULTS

Fig. 1 shows the results of measurements on photographs of a large number of individual spermatozoa at various Ca^{2+} concentrations. Bend angles were measured independently for principal bends (θ_P) and reverse bends (θ_R) by measuring the angles between "straight regions" on either side of a bend, which are effectively represented by a line which appears to be tangent to the arcs of two adjacent bends (4). Principal bends lie on the outside of the curved swimming path of a spermatozoon, have the same sense as the curvature of the swimming path, and are usually larger in angle than the reverse bends in the opposite direction (17). Although principal and reverse bends have opposite sign, θ_P and θ_R will be used here as positive measures of the absolute values of their angles. The mean bend angle is therefore (θ_P +

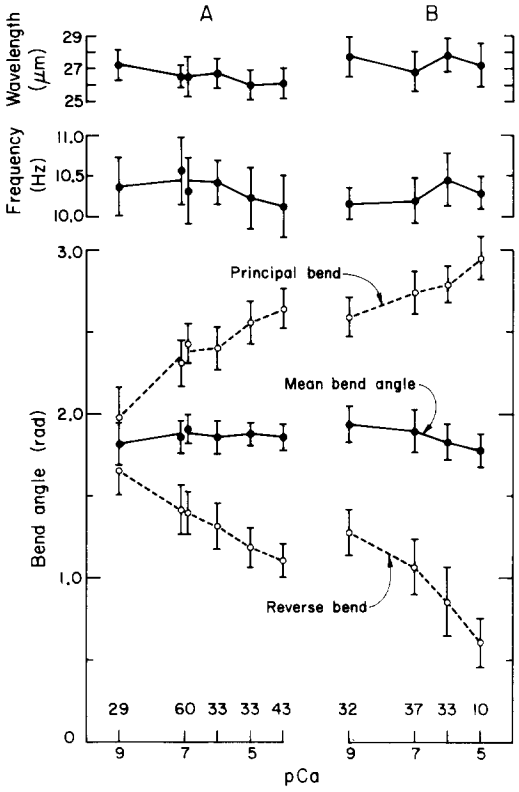

FIGURE 1 Effect of Ca^{2+} concentration on parameters of movement of demembranated flagella. Results for spermatozoa demembranated with Triton solutions containing 2 mM $CaCl_2$ are shown in A; results for spermatozoa demembranated with Triton solutions without $CaCl_2$ are shown in B. Results were obtained with two different sperm samples, which gave significantly different degrees of asymmetry. The values shown are the mean values for the means and standard deviations obtained with each sperm sample. The total number of spermatozoa measured at each Ca^{2+} concentration is indicated at the bottom of the figure. In A, the points at pCa = 7 represent results obtained with reactivation solutions containing 2 mM EGTA, on the left, and 2 mM EDTA, on the right. (pCa indicates a Ca^{2+} concentration of 10^{-pCa} M.)

$\theta_R)/2$, and $\Delta\theta = \theta_P - \theta_R$ is a useful measure of the degree of asymmetry.

These experiments show that the effect of Ca^{2+} concentration on beat frequency, mean bend angle, and wavelength is small or insignificant, in contrast to the large effect of Ca^{2+} on the symmetry of beating. There is a gradual increase in $\Delta\theta$ with increasing Ca^{2+} concentration, and larger values of $\Delta\theta$ are obtained at each Ca^{2+} concentration when $CaCl_2$ is omitted from the Triton solution used for demembranating the spermatozoa. These results agree with earlier results in which the turning rate of the swimming paths of spermatozoa was used as a measure of asymmetry (12). Different sperm samples commonly gave different degrees of asymmetry. For instance, one of the two sperm samples used to obtain the results shown in Fig. 1 gave a $\Delta\theta$ value of 0.17 radians when demembranated in the presence of 2 mM $CaCl_2$ and reactivated at pCa = 9; while the other sperm sample gave a $\Delta\theta$ value of 0.47 radians under the same conditions. This difference in the $\Delta\theta$ values of the two samples was maintained over the range of Ca^{2+} concentrations examined.

Examples of photographic records obtained with moving-film flash photography are shown in Figs. 2, 7, and 9. Data were obtained from photographs at flash rates of 60, 80, or 100 Hz, corresponding to a range of 5.5–11 flashes per beat, and up to 110 flashes per photograph. The first step in analysis of each image was establishment of a baseline corresponding to the centerline of the head. This was easily done when the films were projected on the screen of the microfilm reader, but the prints presented here have been printed to enhance the image of the flagellum, so that the details of the head image are obscured. The head centerline was taken to be the best available measure of the orientation of the basal end of the flagellum (19). The angle of each "straight region" between bends along the flagellum was measured relative to this baseline, and recorded. These measurements, or the measurements of angles in principal and reverse bends derived from them, were then plotted to give graphs of angles as a function of time. These graphs were then used to obtain the beat frequency and average values for bend angle as a function of time in the beat cycle (4), leading finally to graphs such as Fig. 3. In this case, the flash frequency was 10.25 times the beat frequency, and the results represent an average over eight beat cycles. The graphs show the bend angle in the principal and reverse bends as a function of time as each bend develops and propagates along the flagellum. As shown in Fig. 3, two straight lines were fitted by eye to the points for each bend: a horizontal line representing the final bend angles, θ_P and θ_R, and sloping lines approximating the development of these bends. The angle between the baseline for each image and a fixed direction was also measured as a function of time to obtain the turning rate of the swimming path of the spermatozoon. Fig. 4 shows the correlation

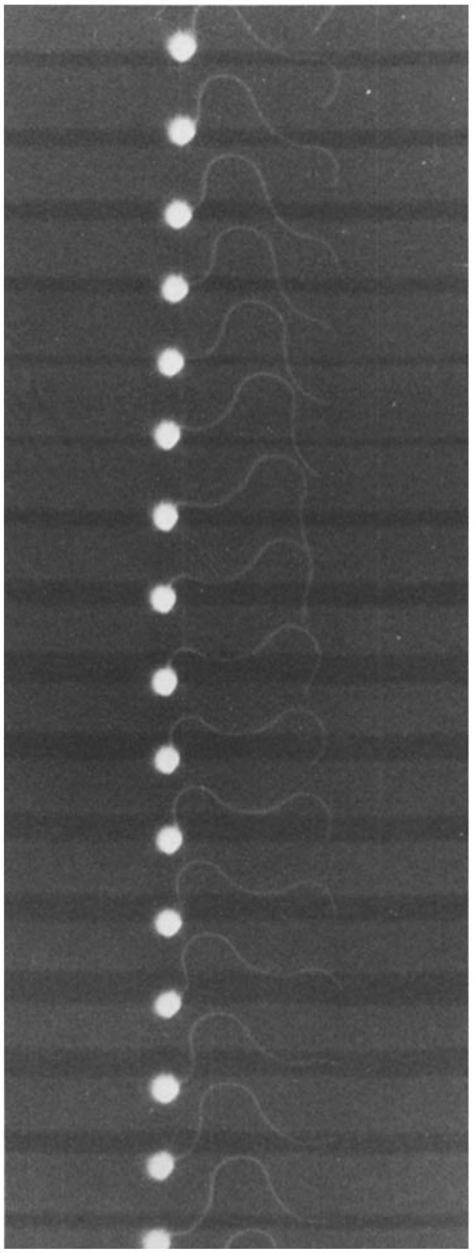

FIGURE 2 A portion of the photographic record of the movement of a sea urchin spermatozoon after demembranation in the presence of 2 mM $CaCl_2$ and reactivation at pCa = 4. The flash frequency was 100 Hz.

between turning rate measured in this manner and asymmetry, $\Delta\theta$. A similar correlation was found with live echinoderm spermatozoa (19), using a slightly different measure of turning rate. Since there are relatively large variations in asymmetry among individual spermatozoa and different sperm samples, subsequent analysis will be referred to the degree of asymmetry, measured by $\Delta\theta$, rather than to Ca^{2+} concentration.

Fig. 3 illustrates the main features shown by bend angle graphs of asymmetrical flagellar waveforms. Asymmetry in bend angle, $\Delta\theta$, is the result

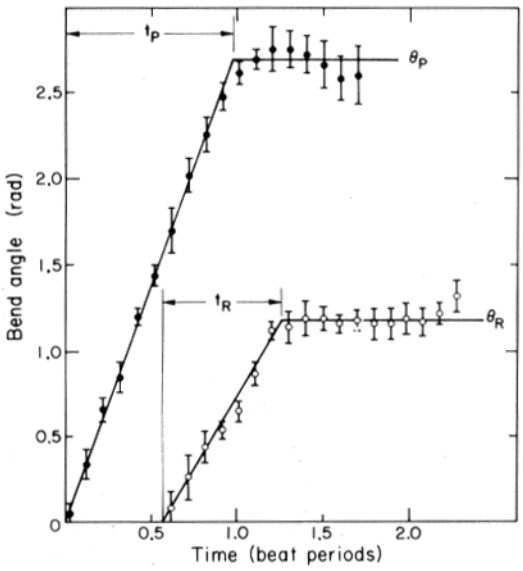

FIGURE 3 Results of bend angle measurements for the spermatozoon shown in Fig. 2. Standard deviations are shown for the eight measurements of bend angle obtained at each time point in the beat cycle. The solid points identify measurements on the principal bends and the open points identify measurements on the reverse bends. Although the principal and reverse bends have opposite sign, the absolute values of bend angle are shown in this figure for the sake of compactness.

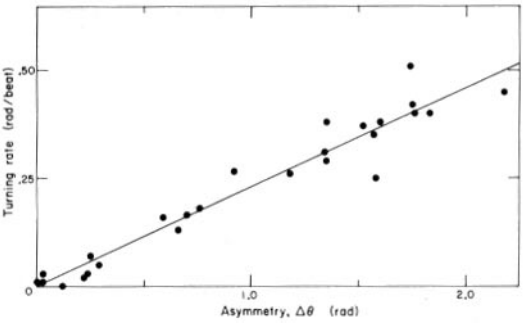

FIGURE 4 Comparison of measured values of turning rate and asymmetry for 26 spermatozoa at various pCa values. The line was obtained by the method of least squares, and has an intercept of 0.0005 radians. The correlation coefficient is 0.97.

of two modifications of the pattern of bend initiation described previously (18; see also Fig. 2 of reference 11) for symmetrical waveforms. The principal bend develops at a greater rate, and over a longer time period, than the reverse bend. This can be described by

$$\Delta\theta = \theta_P - \theta_R = \dot{\theta}_P t_P - \dot{\theta}_R t_R, \qquad (1)$$

where $\dot{\theta}_P$ and $\dot{\theta}_R$ are the linear approximations to the growth rates of the principal and reverse bends, respectively, and t_P and t_R are the durations of the growth periods of the principal and reverse bends, respectively, measured relative to the period of one beat cycle.

Fig. 5 shows the values of t_P and t_R obtained for a sample of 26 spermatozoa analyzed in this manner. For spermatozoa with symmetrical, or nearly symmetrical, waveforms, the values of t_P and t_R are close together, and usually slightly less than 1.0. For flagella with asymmetrical waveforms, the values of t_P typically remain near 1.0, although one case with a much larger value of t_P (1.39) was found (see Fig. 3 of reference 11). The values of t_R for asymmetrical waveforms are significantly less than 1.0, and decrease slightly with increasing asymmetry. The growth of the reverse bend terminates well before initiation of a new reverse bend, so that there is a significant period in which only the principal bend is developing near the basal end of the flagellum. As noted by Goldstein (19), this requires a significant alteration in the pattern of sliding between microtubules in distal regions of the flagellum.

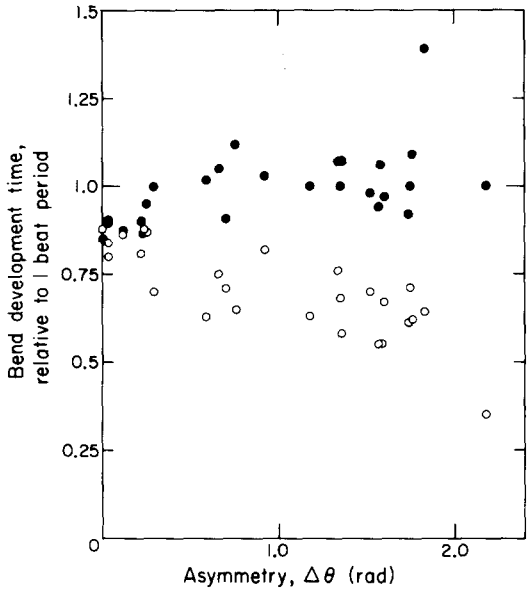

FIGURE 5 Relationship between bend development time and asymmetry for 26 spermatozoa at various pCa values. The solid circles represent t_P, the time for development of a principal bend, and the open circles represent t_R, the time for development of a reverse bend. These quantities are defined as illustrated in Fig. 3.

The asymmetry can be considered to be caused by two factors: the presence in the beat cycle of a significant period during which only the principal bend is developing, to cause a difference in angle equal to $\dot{\theta}_P(t_P - t_R)$ and the difference in growth rates during the portion of the beat cycle during which both bends are developing, to cause a difference in angle equal to $t_R(\dot{\theta}_P - \dot{\theta}_R)$. This can then be described by

$$\Delta\theta = \Delta_t + \Delta_{\dot{\theta}} = \dot{\theta}_P(t_P - t_R) + t_R(\dot{\theta}_P - \dot{\theta}_R), \quad (2)$$

where Δ_t represents the asymmetry resulting from growth of the principal bend after the reverse bend stops growing, and $\Delta_{\dot{\theta}}$ represents the asymmetry resulting from the difference in growth rates of the principal and reverse bends during the time both bends are developing. It can be easily verified that equations *1* and *2* are equivalent.

Fig. 6 summarizes the contributions of Δ_t and $\Delta_{\dot{\theta}}$ to the asymmetry of the spermatozoa in the sample studied. It shows that Δ_t is the dominant factor, and that the role of $\Delta_{\dot{\theta}}$ is more variable, at least at lower values of asymmetry. Point A in Fig. 6 represents a spermatozoon for which $\Delta_{\dot{\theta}}$ is almost

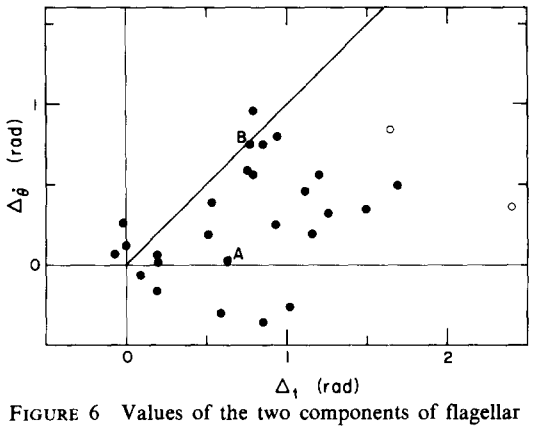

FIGURE 6 Values of the two components of flagellar asymmetry, $\Delta_{\dot{\theta}}$ and Δ_t, defined in the text. Point B corresponds to the flagellum shown in Figs. 2 and 3. The two open circles correspond to flagella showing more extreme asymmetry, involving a decrease in the reverse bend angle; the point at the far right corresponds to the flagellum shown in Figs. 7 and 8.

0, and the asymmetry is due almost entirely to Δ_t. There are no examples where a similarly large asymmetry is due almost entirely to $\Delta_{\dot{\theta}}$.

When the asymmetry is more extreme, as exemplified by the spermatozoon shown in Fig. 7, the angle of the reverse bend usually decreases as the bend propagates, and the measurement of θ_R, and sometimes θ_P, is ambiguous. Bend angle curves for the spermatozoon shown in Fig. 7 are given in Fig. 8. In this case, there is a period of 0.6 cycle during which only the principal bend is growing, with a high rate of 4.0 radians per cycle, resulting in $\Delta_t = 2.4$ radians. During the remaining 0.4 cycle, in which both bends are growing, there is an additional increase in asymmetry of 0.36 radians, which corresponds to $\Delta_{\dot{\theta}}$. Points for this flagellum and a similar example are shown by open circles in Fig. 6.

Moving film flash photography can also be used to look for changes in asymmetry when the mean bend angle is reduced by exposing the spermatozoa to CO_2 (9, 14), but the quality of the images is less because an open drop preparation and an objective of lower aperture must be used. Fig. 9 shows an example of the results obtained from this type of experiment. The beat cycle shown in the left strip is similar to earlier beat cycles recorded on the film, but not shown here. In subsequent beat cycles, there is an obvious reduction in bend angles of both principal and reverse bends with relatively little change in beat frequency or in asymmetry, $\theta_P - \theta_R$. This type of observation complements the results shown in Fig. 1 and provides additional evidence for independent mechanisms controlling asymmetry and other wave parameters. The flagella usually come to rest in a curved configuration, as shown in the last two images, but the rest configurations obtained with CO_2-inhibition are variable, and are sometimes almost straight.

Analysis of Shear Between Tubules

The bend angle curves shown in Figs. 3 and 8 give only a partial description of the behavior of these flagella. A more complete and useful description would be provided by curves showing the amount of sliding between tubules as a function of length along the flagellum. If no shear displacement between tubules is allowed at the basal end of the flagellum, then an angular measure of the shear displacement between tubules at a point, s, along the length is given by the angle between tangents to the flagellum at s and at the base (31).

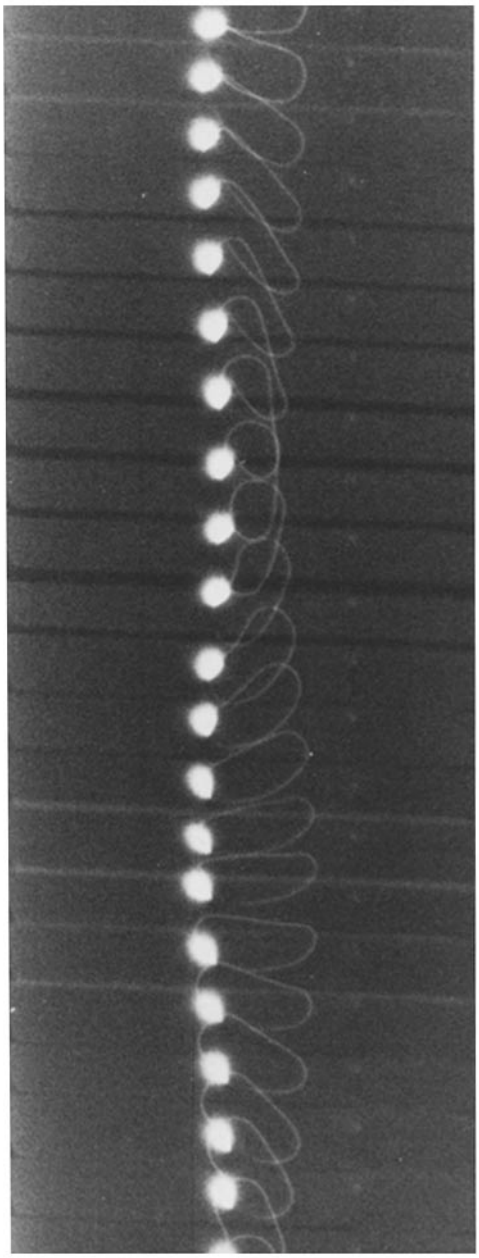

FIGURE 7 A portion of the photographic record of the movement of a sea urchin spermatozoon after demembranation without addition of $CaCl_2$ to the Triton solution and reactivation at pCa = 4. The flash frequency was 100 Hz.

Methods for determining these angles from photographs of flagella have been described (21, 32). I have found it more convenient to trace the photographic images onto paper, and then to fit as

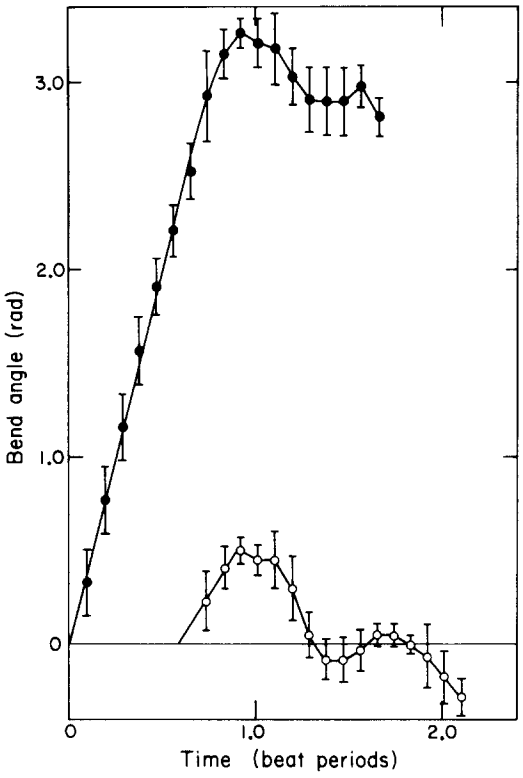

FIGURE 8 Results of bend angle measurements for the spermatozoon shown in Fig. 7, represented as in Fig. 3. Each point represents measurements averaged for nine consecutive beat cycles.

much of the waveform as possible with circular arcs and straight lines (2, 4). This is not an unbiased method for obtaining information about the shapes of the curves, but is an accurate method for measuring the positions of bends on a flagellum. It is still a highly time-consuming method which is not practical to use for analysis of all of the large number of images available from the moving-film photography. A complete analysis of these photographs must await development of more automated and precise methods than those which are currently available. Shear curves which I have obtained from a partial analysis of the asymmetrically beating flagellum shown in Fig. 7 are shown in Fig. 10.

Inspection of shear curves of asymmetrically beating flagella provides the following information: (*a*) An asymmetrical waveform is characterized by a gradual deviation of the centerline of the envelope of the shear curves from the line of 0 shear. (*b*) As noted previously (19), the lengths of principal and reverse bends on asymmetrically beating flagella remain approximately equal, while the bend angles and curvatures of principal and reverse bends are unequal. (*c*) In the asymmetrically beating flagella examined here, there is always a constriction of the envelope of the shear curves near the mid-region of the flagellum. Relative to symmetrical waves, the amplitude and rate of sliding are decreased in this mid-region and increased in other regions of the flagellum. (*d*) In extreme cases, such as shown in Fig. 10, the shear curves show that during a portion of the beat cycle when only a principal bend is developing at the basal end of the flagellum, the propagating principal bend is a region in which the rate of sliding between tubules (indicated by the vertical separation between the shear curves) is very low. During another portion of the beat cycle, the rate of sliding in the propagating reverse bend is very low. However, the bends continue to propagate regularly in spite of these large variations in sliding rates within the bends (19).

DISCUSSION

Active bending by flagella and cilia has been shown to be the result of an ATP-driven active sliding process which operates between the outer doublet microtubules of the axoneme (5, 33). This active sliding process appears to involve the dynein arms, which can form stable cross-bridges between microtubules under some conditions, and which may generate active sliding by an attachment-detachment cycle similar to that suggested for the actin-myosin system (8). The action of dynein arms appears to be unidirectional (30). Because of their arrangement around the periphery of the axoneme, arms on opposite sides of the axoneme will act antagonistically with respect to bending, so that simultaneous activation of all the arms in an intact axoneme will presumably cause little bending. For efficient bending, it appears that only half of the dynein arms, only those located on one side of the axoneme, should be activated at any one time.

Within a bend propagating along the distal portion of a symmetrically beating flagellum, tubules should be sliding uniformly in one direction, and, presumably, only the dynein arms on one side of the axoneme should be activated. This pattern, in which a region of active shear in one direction travels along with a propagating bend, has been referred to as metachronous sliding or metachronous activation (10, 18). Most recent attempts to design mechanisms for oscillation and

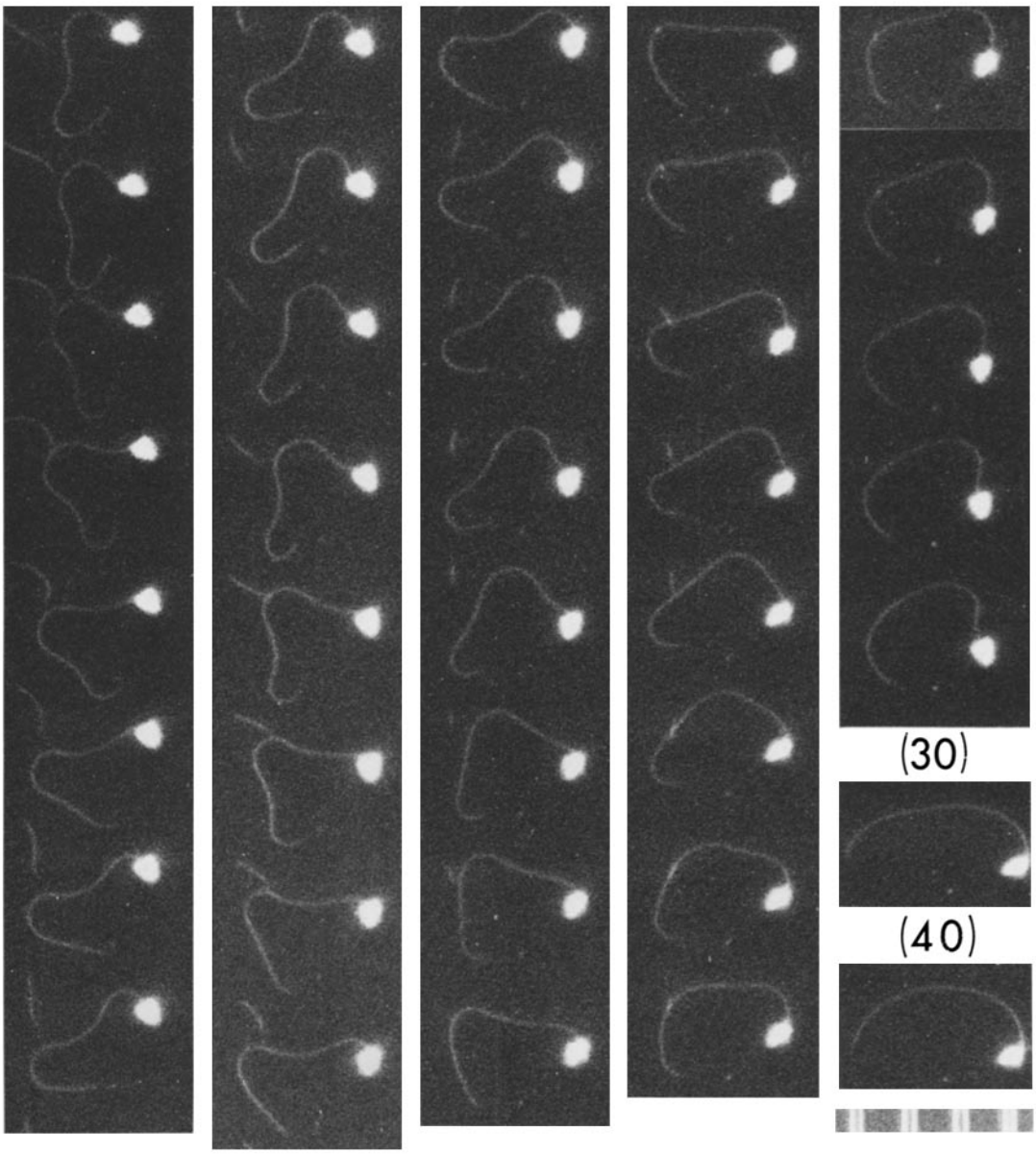

FIGURE 9 Movement of a sea urchin spermatozoon during exposure to CO_2 in a reactivation solution at pCa = 4, after demembranation in the presence of 2 mM $CaCl_2$. The exact time course of exposure to CO_2 was not recorded, but the first effects can probably be detected during the second beat cycle shown here (the second vertical strip). The flash frequency was 60 Hz; the scale divisions are 10 μm; and the numbers above the last two frames indicate the number of frames omitted.

bend propagation in flagella and cilia have focused on mechanisms for appropriately controlling the active shear process (6, 13, 20, 24, 28, 29). Computations with flagellar models in which metachronous activation is achieved by a feedback control of cross-bridge kinetics by curvature have demonstrated the ability of this kind of simple control mechanism to generate oscillation and bend propagation (13, 20). If these ideas about the control of metachronous sliding are valid, they should also

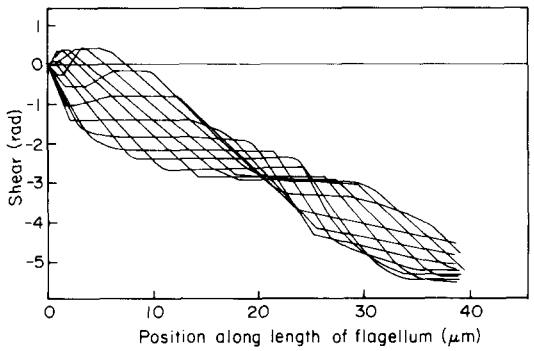

FIGURE 10 Shear curves obtained from the photograph shown in Fig. 7. Each curve is the average of two curves obtained in successive beat cycles. There are 11 superimposed curves covering equally-spaced images in one beat cycle. Shear is measured by the angle between the head centerline and a tangent to the flagellum at a point along its length. A horizontal line represents a straight region between bends; the difference in shear between two straight regions on either side of a bend is a measure of the bend angle of that bend. A straight line inclined at an angle in this figure represents a circular arc approximation of a bend in the original photograph. A principal bend is assigned a negative curvature, and is represented by a line of negative slope in this figure.

provide a basis for understanding the control of asymmetrical flagellar bending waves and the various types of asymmetrical bending patterns exhibited by cilia.

The present work provides evidence that the parameters of metachronous sliding and the degree of asymmetry are independent of each other. The observation that both frequency and mean bend angle remain constant as the degree of asymmetry is changed by changing the Ca^{2+} concentration implies that both the rate and amplitude of metachronous sliding remain constant. The main feature of asymmetrical bending waves is a displacement of the center-point of this oscillatory sliding, which gradually increases toward the distal end of the flagellum. This could represent simply a curvature of the flagellar axis, on which a normal pattern of symmetrical metachronous sliding is superimposed. If this curvature of the flagellar axis is uniform, so that the "rest position" of the flagellum is circular rather than straight, the curvature of principal bends will be uniformly increased and the curvature of reverse bends will be uniformly decreased. The resulting asymmetry will be purely $\Delta_{\dot{\theta}}$ asymmetry. This type of explanation is attractive, because it is easy to imagine how an independent curvature of the flagellum could be caused by an independent contractile mechanism, possibly related to the calcium-driven contractile mechanism of the ciliate spasmoneme (1). However, this explanation is obviously insufficient, because it fails to explain the Δ_t asymmetry which has been found to be a significant component of asymmetrical flagellar bending patterns, and because it fails to explain how a curvature-controlled mechanism for metachronous oscillation could be insensitive to the additional curvature of the flagellum associated with asymmetrical bending waves.

An alternative view is that the curvature of the flagellar axis which is characteristic of asymmetrical bending waves is the result of the propagation of unequal principal and reverse bends. For example, if metachronous activation is controlled by a mechanism which switches activity from one side of the flagellum to the other when a critical curvature is attained, asymmetrical bending waves could be generated if the critical curvatures for switching were different for the two directions of bending. Such an explanation is also insufficient, because it fails to explain the constant magnitude of the mean bend angle, and because in its simplest form it would also be expected to generate only $\Delta_{\dot{\theta}}$ asymmetry.

The generation of Δ_t asymmetry requires a modification of the pattern of metachronous sliding which can be described as a superposition of synchronous and metachronous sliding. Synchronous sliding is sliding at a uniform rate throughout a length of flagellum. It can cause no bending within the region of uniform sliding. Completely synchronous sliding throughout the length of an intact flagellum is impossible, because sliding between the tubules is restricted at the basal end of the flagellum (31, 33, 35). In the present context, synchronous sliding means sliding at a uniform rate in distal regions of the flagellum, beyond the two bends which are developing near the base of the flagellum, and its magnitude is equal to the difference between the absolute values of $\dot{\theta}_P$ and $\dot{\theta}_R$. In a flagellum showing only Δ_t asymmetry, the time at which the reverse bend stops growing represents a time at which there is a transition from a state in which the magnitudes of $\dot{\theta}_P$ and $\dot{\theta}_R$ are equal and there is no synchronous sliding to a state in which only the principal bend is growing, with synchronous sliding throughout the remainder of the flagellum. In many cases, this transition appears to

be abrupt, and is reminiscent of the abrupt onset of synchronous sliding at the beginning of the effective stroke of a cilium.

Synchronous sliding is probably not the cause of Δ_t asymmetry. Fig. 11 *c* illustrates the pattern of sliding for a hypothetical flagellar waveform showing only Δ_t asymmetry. In this case, $t_P = 1.0$ and $t_R = 0.5$, and the reverse bend angle decreases to 0 during the period from 0.5 to 1.0 cycles after initiation of its growth. This waveform is generated by a combination of a metachronous shear oscillation, which by itself would produce the pattern shown in Fig. 11 *a*, and a synchronous shear oscillation. The synchronous shear oscillation is symmetrical—it involves sliding in one direction for 0.5 cycles and then in the other direction for 0.5 cycles. The phase relationship is such that the synchronous sliding always adds to the growth of the bend nearest the base of the flagellum. The magnitudes of synchronous and metachronous sliding are equal, and they therefore cancel each other out at points on the flagellum where the oscillations are ½-cycle out of phase. This hypothetical waveform has been designed to reproduce the main features of the flagellar shear pattern shown in Fig. 10. Fig. 11 *b* illustrates another waveform generated by the same combination of metachronous and synchronous sliding in the distal regions of the flagellum (e.g., beyond the first two bend regions). In this case, both t_P and $t_R = 0.5$ cycles. The synchronous sliding in this waveform causes the same constriction of the envelope of the shear curves commonly seen with asymmetrical waveforms, but does not cause asymmetry. The most obvious effect on the waveform is to cause the orientation of the head end of the flagellum to oscillate with respect to the centerline of the waveform, in contrast to Fig. 11 *a*. The difference between the waveforms in Fig. 11 *c* and 11 *b* is equivalent to a fixed curvature of the flagellar axis beginning somewhat beyond the region of the first bend and therefore causing no $\Delta_{\dot{\theta}}$ asymmetry. In general, synchronous sliding appears to be required whenever t_P or t_R is unequal to 1.0 and therefore must occur if t_P is unequal to t_R, but it is not sufficient to generate Δ_t asymmetry and does not generate $\Delta_{\dot{\theta}}$ asymmetry. The most interesting feature of synchronous sliding is that it appears to have little or no effect on the propagation of bends in the distal region of the flagellum (19).

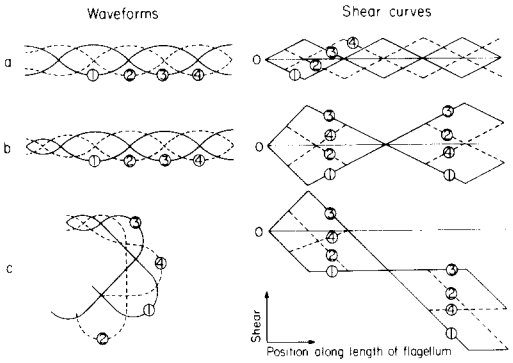

FIGURE 11 Some hypothetical flagellar waveforms and their shear curves. The basal end of each flagellum is on the left. These waveforms consist entirely of circular arcs of constant curvature, with no "straight regions" between bends. There is no sliding in the first bend. Each pattern contains four curves at equally spaced time intervals covering one beat cycle. The relative positions of the waveforms are not the result of hydrodynamic calculations and do not portray the propulsion of the flagellum.

The mean bend angle, wavelength, and propagation velocities are the same for each waveform. Waveform a is generated entirely by metachronous sliding. Waveforms b and c are generated by addition of synchronous sliding to the patterns shown in a. The synchronous sliding is apparent when the shear curves at times 1 and 3 of patterns a and b are compared. The shear at time 1 is uniformly decreased in the distal portion of the flagellum in b relative to a, and at time 3 it is increased.

This discussion has highlighted some of the difficulties involved in trying to find a simple perturbation of flagellar control mechanisms by Ca^{2+} which will explain the occurrence of both Δ_t and $\Delta_{\dot{\theta}}$ asymmetry, in variable proportions, in asymmetrical flagellar bending patterns and the apparent insensitivity of the mechanism which controls the metachronous sliding associated with symmetrical bending waves to the changes in curvature and rates of sliding between tubules which are found in asymmetrical bending patterns. At this stage, it appears that the simple control mechanisms which have been suggested for metachronous activation in symmetrical bending waves fail to provide a satisfactory basis for understanding the generation of asymmetrical bending patterns. This conclusion certainly dictates caution in assuming that these simple control mechanisms really operate in flagella to generate symmetrical bending waves, in spite of the successful generation of bending waves by theoretical models incorporating these simple control mechanisms.

I thank Tom Simonick for able technical assistance with this work, and S. F. Goldstein, I. R. Gibbons, and P. Satir for valuable suggestions.

This work was supported by National Institutes of Health (NIH) grant GM-18711 and by grant RR07003 awarded by the Biomedical Research Support Grant program, Division of Research Resources, NIH.

Received for publication 11 December 1978, and in revised form 1 March 1979.

REFERENCES

1. AMOS, W. B. 1975. Contraction and calcium binding in the vorticellid ciliates. *In* Molecules and Cell Movement. S. Inoue and R. E. Stephens, editors. Raven Press, N. Y. 411–435.
2. BROKAW, C. J. 1965. Non-sinusoidal bending waves of sperm flagella. *J. Exp. Biol.* **43**:155–169.
3. BROKAW, C. J. 1966. Effects of increased viscosity on the movements of some invertebrate spermatozoa. *J. Exp. Biol.* **45**:113–139.
4. BROKAW, C. J. 1970. Bending moments in free-swimming flagella. *J. Exp. Biol.* **53**:445–464.
5. BROKAW, C. J. 1972. Flagellar movement: a sliding filament model. *Science (Wash. D. C.).* **178**:455–462.
6. BROKAW, C. J. 1972. Computer simulation of flagellar movement. I. Demonstration of stable bend propagation and bend initiation by the sliding filament model. *Biophys. J.* **12**:564–586.
7. BROKAW, C. J. 1975. Effects of viscosity and ATP concentration on the movement of reactivated sea urchin sperm flagella. *J. Exp. Biol.* **62**: 701–719.
8. BROKAW, C. J. 1975. Cross-bridge behavior in a sliding filament model for flagella. *In* Molecules and Cell Movement. S. Inoue and R. E. Stephens, editors. Raven Press, N. Y. 165–178.
9. BROKAW, C. J. 1977. CO_2-inhibition of the amplitude of bending of triton-demembranated sea urchin sperm flagella. *J. Exp. Biol.* **71**:229–240.
10. BROKAW, C. J., and I. R. GIBBONS. 1975. Mechanisms of movement in flagella and cilia. *In* Swimming and Flying in Nature. T. Y.-T. Wu, C. J. Brokaw, and C. Brennan, editors. Plenum Publishing Corp., N. Y. **1**: 89–126.
11. BROKAW, C. J., and S. F. GOLDSTEIN. 1979. Asymmetrical oscillation of sea urchin sperm flagella induced by calcium. *In* The Spermatozoon: Maturation, Motility and Surface Properties. D. W. Fawcett and J. M. Bedford, editors. Urban and Schwarzenberg, Baltimore, Md. In press.
12. BROKAW, C. J., R. JOSSLIN, and L. BOBROW. 1974. Calcium ion regulation of flagellar beat symmetry in reactivated sea urchin spermatozoa. *Biochem. Biophys. Res. Commun.* **58**:795–800.
13. BROKAW, C. J., and D. RINTALA. 1975. Computer simulation of flagellar movement. III. Models incorporating cross-bridge kinetics. *J. Mechanochem. Cell Motility.* **3**:77–86.
14. BROKAW, C. J., and T. F. SIMONICK. 1976. CO_2 regulation of the amplitude of flagellar bending. *In* Cell Motility. R. Goldman, T. Pollard, and J. Rosenbaum, editors. Cold Spring Harbor Laboratory, Cold Spring Harbor, N. Y. 933–940.
15. BROKAW, C. J., and T. F. SIMONICK. 1977. Mechanochemical coupling in flagella. V. Effects of viscosity on movement and ATP-dephosphorylation of Triton-demembranated sea urchin spermatozoa. *J. Cell Sci.* **23**:227–241.
16. BROKAW, C. J., and T. F. SIMONICK. 1977. Motility of triton-demembranated sea urchin sperm flagella during digestion by trypsin. *J. Cell Biol.* **75**:650–665.
17. GIBBONS, B. H., and I. R. GIBBONS. 1972. Flagellar movement and adenosine triphosphatase activity in sea urchin sperm demembranated with Triton X-100. *J. Cell Biol.* **54**:75–97.
18. GOLDSTEIN, S. F. 1976. Form of developing bends in reactivated sperm flagella. *J. Exp. Biol.* **64**:173–184.
19. GOLDSTEIN, S. F. 1977. Asymmetric waveforms in echinoderm sperm flagella. *J. Exp. Biol.* **71**:157–170.
20. HINES, M., and J. J. BLUM. 1979. Bend propagation in flagella. II. Incorporation of dynein cross-bridge kinetics into the equations of motion. *Biophys. J.* **25**:421–442.
21. HIRAMOTO, Y., and S. A. BABA. 1978. A quantitative analysis of flagellar movement in echinoderm spermatozoa. *J. Exp. Biol.* **76**:85–104.
22. HOLWILL, M. E. J., and J. L. MCGREGOR. 1975. Control of flagellar wave movement in *Crithidia oncopelti. Nature (Lond.).* **255**:157–158.
23. HYAMS, J., and G. BORISY. 1978. Isolated flagellar apparatus of Chlamydomonas: characterization of forward swimming and alteration of waveform and reversal of motion by calcium ions *in vitro*. *J. Cell Sci.* **33**:235–254.
24. LUBLINER, J., and J. J. BLUM. 1972. Analysis of form and speed of flagellar waves according to a sliding filament model. *J. Mechanochem. Cell Motility.* **1**:157–167.
25. MACHEMER, H. 1977. Motor activity and bioelectric control of cilia. *Fortschr. Zool.* **24**:195–210.
26. MILLER, R. L., and C. J. BROKAW. 1970. Chemotactic turning behavior of *Tubularia* spermatozoa. *J. Exp. Biol.* **52**:699–706.
27. NAITOH, Y., and H. KANEKO. 1972. Reactivated triton-extracted models of *Paramecium*: modification of ciliary movement by calcium ions. *Science (Wash. D. C.).* **176**:523–524.
28. RIKMENSPOEL, R. 1971. Contractile mechanisms in flagella. *Biophys. J.* **11**:446–463.
29. RIKMENSPOEL, R., and W. G. RUDD. 1973. The contractile mechanism in cilia. *Biophys. J.* **13**:955–993.
30. SALE, W. S., and P. SATIR. 1977. Direction of active sliding of microtubules in *Tetrahymena* cilia. *Proc. Natl. Acad. Sci. U. S. A.* **74**:2045–2049.
31. SATIR, P. 1968. Studies on cilia. III. Further studies of the cilium tip and a "sliding filament" model of ciliary motility. *J. Cell. Biol.* **39**:77–94.
32. SILVESTER, N., and D. JOHNSTON. 1976. An electro-optical curve follower with analog control. *J. Phys. E. Sci. Instrum.* **9**:990–995.
33. SUMMERS, K. E., and I. R. GIBBONS. 1971. Adenosine triphosphate-induced sliding of tubules in trypsin-treated flagella of sea-urchin sperm. *Proc. Natl. Acad. Sci. U. S. A.* **68**:3092–3096.
34. TSUCHIYA, T. 1977. Effects of calcium ions on triton-extracted lamellibranch gill cilia: ciliary arrest response in a model system. *Comp. Biochem. Physiol. A Comp. Physiol.* **56**:353–361.
35. WARNER, F. D., and P. SATIR. 1974. The structural basis of ciliary bend formation. Radial spoke positional changes accompanying microtubule sliding. *J. Cell Biol.* **63**:35–63.